Published online 4 June 2021 *Nucleic Acids Research, 2021, Vol. 49, No. 20* ***11629–11642***
https://doi.org/10.1093/nar/gkab460

Human MettL3-MettL14 RNA adenine methyltransferase complex is active on double-stranded DNA containing lesions

Dan Yu[1,†], John R. Horton[1,†], Jie Yang[1], Taraneh Hajian[2], Masoud Vedadi[2,3], Cari A. Sagum[1], Mark T. Bedford[1], Robert M. Blumenthal[4,*], Xing Zhang[1,*] and Xiaodong Cheng[1,*]

[1]Department of Epigenetics and Molecular Carcinogenesis, University of Texas MD Anderson Cancer Center, Houston, TX 77030, USA, [2]Structural Genomics Consortium, University of Toronto, Toronto, ON Canada, [3]Department of Pharmacology and Toxicology, University of Toronto, Toronto, ON M5S 1A8, Canada and [4]Department of Medical Microbiology and Immunology, and Program in Bioinformatics, The University of Toledo College of Medicine and Life Sciences, Toledo, OH 43614, USA

Received April 10, 2021; Revised May 07, 2021; Editorial Decision May 11, 2021; Accepted May 13, 2021

ABSTRACT

MettL3-MettL14 methyltransferase complex has been studied widely for its role in RNA adenine methylation. This complex is also recruited to UV- and X-ray exposed DNA damaged sites, and its methyltransfer activity is required for subsequent DNA repair, though in theory this could result from RNA methylation of short transcripts made at the site of damage. We report here that MettL3-MettL14 is active *in vitro* on double-stranded DNA containing a cyclopyrimidine dimer – a major lesion of UV radiation-induced products – or an abasic site or mismatches. Furthermore, N6-methyladenine (N6mA) decreases misincorporation of 8-oxo-guanine (8-oxoG) opposite to N6mA by repair DNA polymerases. When 8-oxoG is nevertheless incorporated opposite N6mA, the methylation inhibits N6mA excision from the template (correct) strand by the adenine DNA glycosylase (MYH), implying that the methylation decreases inappropriate misrepair. Finally, we observed that the N6mA reader domain of YTHDC1, which is also recruited to sites of DNA damage, binds N6mA that is located across from a single-base gap between two canonical DNA helices. This YTHDC1 complex with a gapped duplex is structurally similar to DNA complexes with FEN1 and GEN1 – two members of the nuclease family that act in nucleotide excision repair, mismatch repair and homologous recombination, and which incise distinct non-B DNA structures. Together, the parts of our study provide a plausible mechanism for N6mA writer and reader proteins acting directly on lesion-containing DNA, and suggest *in vivo* experiments to test the mechanisms involving methylation of adenine.

INTRODUCTION

Genomic DNA is continually subject to damage from insults that range from UV irradiation or (aging-associated) oxidative stress, to interactions with environmental mutagens and cancer chemotherapeutic drugs (1). Interestingly, upon UV irradiation of human sarcoma U2OS cells pretreated with bromodeoxyuridine, the MettL3-MettL14 RNA methyltransferase complex (termed MettL3-14 hereafter) is recruited within 2 min to the damaged sites, and MettL3 catalytic activity is required for subsequent DNA repair (2). Further, repair-associated DNA polymerase κ requires the catalytic activity of MettL3 for its immediate localization to sites of DNA damage (2). In another study (also in human sarcoma U2OS cells), irradiation with X-rays or treatment with chemicals that induce double-strand breaks (DSBs) leads to colocalization of MettL3 with the phosphorylated histone variant γH2A.X (3).

MettL3-14 methyltransferase complex has been studied widely for its role in generating N6-methyladenine (N6mA) in RNA (4–6), at the degenerate consensus sequence RRACH (R = purine and H = not G) (7). Because the functional role of RNA modifications may be both site specific and RNA-species specific, an RNA-associated DNA repair mechanism has been suggested (2,3), but the

*To whom correspondence should be addressed. Email: XCheng5@mdanderson.org
Correspondence may also be addressed to Xing Zhang. Email: XZhang21@mdanderson.org
Correspondence may also be addressed to Robert M. Blumenthal. Email: Robert.Blumenthal@utoledo.edu
†The authors wish it to be known that, in their opinion, the first two authors should be regarded as Joint First Authors.

involvement of (RNA) methylation has not been demonstrated directly in the steps along the pathways of either nucleotide excision repair (NER) or DSB repair (which is complex in somatic mammalian cells (8)).

In addition to its enrichment at the 3′ end of protein-coding genes, consistent with its involvement in mRNA adenine methylation, MettL3 also localizes to the transcriptional start sites of active genes (through association with transcription factor CEBPζ) (9). Moreover, MettL3-14, its methylated RNA products, or the N6mA reader protein YTHDC1 are associated with chromatin having histone modification marks that varied case-by-case, including H3 lysine 4 trimethylation (H3K4me3) (10), bivalent H3K4me3 and acetylated H3K27 (6), dimethylated H3K9 (H3K9me2) (11) or trimethylated H3K9 (H3K9me3) (12,13), or trimethylated histone H3 lysine 36 (H3K36me3) (14). Significantly, in relation to our study, MettL3 (alone among known DNA or RNA modifying enzymes) was identified as a direct DNA binder in a recent large-scale profiling of protein-DNA interactions, and this DNA binding was enhanced on DNA containing 5-methylcytosine (15).

More recently, MettL3-catalysed N6mA modification of RNA has been suggested to regulate the fate of endogenous retroviruses (ERVs) in mouse embryonic stem cells, either by associating with heterochromatin during transcription (12,13), or via post-transcriptionally clearing reactive ERV-derived RNA species by recruiting YTHDF to the 5′ untranslated regions (16). It is worth noting the conclusion of Chelmicki *et al*. in partial disagreement with other studies (12,13), that N6mA modified RNA does not strongly colocalize with chromatin modifications (H3K4me3, H3K9me3 and H3K27ac), but rather affects ERV mRNA abundance by accelerating its clearance (16), in agreement with its major effect on mRNA lifetimes (17). Thus, ERVs are silenced during early embryogenesis not only by DNA cytosine methylation (18), and histone lysine methylation (19,20), but also by RNA adenine methylation. However the initiator(s) of this process of epigenetic modifications, which is essential to protecting genome integrity (21), remain largely unknown.

While detected immunochemically as early as 1983 (22), N6mA in mammalian DNA was reported again only in 2016 (23). It was found in embryonic stem cell DNA, with the N6mA enriched in H2A.X deposition regions, where H2A.X is a histone variant typically associated with DNA DSBs. N6mA DNA modification is also elevated in glioblastoma (a disease partially associated with the cumulative effects of high-dose exposure to ionizing radiation, or to chemical carcinogens), but not in normal adult tissues or mammalian cells (24). Recently, the same group that reported the initial discovery in 2016, found that N6mA levels in DNA increase during the development of mouse trophoblast stem cells (which eventually give rise to the placenta). They found the N6mA specifically at regions of stress-induced DNA double helix destabilization (25) – locations of non-B DNA structures (26).

We note that the existence of N6mA in mammalian DNA is currently a controversial issue (27–29). There is debate over whether the low level of DNA N6mA can be accurately detected (without RNA contamination and/or bacterial DNA contamination) using ultrasensitive mass spectrometry, or whether the measurements are being made under the right physiological conditions, at the right times, and in the right tissues and genomic locations (30,31).

The following basic considerations prompted us to ask whether human MettL3-14 also possesses methyl transfer activity on adenines in DNA. First, MettL3-14 is recruited rapidly to sites of DNA damage (2). Second, many nucleic acid-modifying enzymes are able to modify both DNA and RNA (reviewed in (32) and references therein), such as members of the AlkB family (33), Apobec family (34) and Tet dioxygenases (35,36). Third, we have previously reported that MettL3-14 displays *in vitro* methyltransfer activity on short synthetic oligonucleotides of single-strand (ss)DNA, with more than tenfold *greater* catalytic efficiency than for ssRNA under the same conditions (37). In addition, MettL3-14 is active on double-stranded (ds)DNA containing mismatched pairs, though it is inactive on normal Watson-Crick fully-base-paired dsDNA (37). Fourth, the NER and DSB repair pathways involve many intermediate non-B DNA conformations. A set of coordinated NER enzymes recognize a wide range of DNA lesions (including UV radiation-induced products), unwind the DNA and excise a ∼25–30 nucleotide segment of the damaged strand, spanning the site of lesion, and generating a transient ssDNA region before gap-filling synthesis by DNA polymerase(s) and subsequent ligation (38).

Based on these four observations, we asked whether MettL3-14 is active *in vitro* on lesion-containing dsDNA. We also addressed the impact of such DNA methylation on repair by the adenine DNA glycosylase, and the impact on repair of N6mA binding by the reader domain of YTHDC1.

MATERIALS AND METHODS

Protein expression and purification

The recombinant proteins used in this study were characterized previously in our laboratories. These include MettL3-14 (37), MYH (39) and YTHDC1 (residues 345–509) (40).

SAM-dependent methylation assays of MettL3-14

Methylation assays of MettL3-14 on ssDNA or dsDNA oligonucleotides, containing a cyclothymine dimer, abasic sites, mismatches, or controls of fully-paired duplexes, proceeded using a constant set of conditions. Reactions were carried out in a 50 μl mixture containing 0.2 μM MettL3-14, 5 μM substrate (ds) oligos, 20 μM SAM in 50 mM HEPES pH 7.5, 5 mM NaCl and 1 mM DTT (reaction buffer). Reactions were conducted at 22°C for 1–4 min, and 10 μl aliquots of reaction sample were quenched by adding 2.5 μl of trifluoroacetic acid (TFA) to a final concentration of 0.1% (v/v). A 5-μl aliquot of reaction sample was transferred into a low-volume 384-well plate. The methylation reaction by-product SAH was measured using the Promega bioluminescence assay (MTase-Glo™) (41), in

which the SAH is converted into ATP in a two-step reaction, and the ATP is then detected through a luciferase reaction. The luminescence signal was measured by a Synergy 4 multimode microplate reader (BioTek).

The reactions for kinetic parameter determination were conducted under steady state conditions, with 50 nM MettL3-14 and 20 μM SAM in a 20 μl mixture of reaction buffer. Reactions were conducted at 22 °C for 10 min for dsDNA or 5 min for ssDNA. The dependence of the product formation per enzyme molecule on substrate concentration was fitted with the Michaelis-Menten equation using GraphPad Prism 8. The standard deviation associated with the second order substrate specificity constants, k_{cat} and K_m, were calculated using an error of propagation equation.

The oligonucleotides used in assays were synthesized by Integrated DNA Technologies or BioSynthesis (cyclothymine dimer). Double-stranded oligos containing a cyclothymine dimer were generated by annealing with the complementary strand in approximately equimolar ratio (or slightly more TT strand) in 20 mM Tris–HCl pH 7.8 and 100 mM NaCl. All oligonucleotides were visualized on a 15% acrylamide gel (1× Tris–borate–EDTA (TBE), 0.05% ammonium persulfate (APS) and 0.1% tetramethylethylenediamine (TEMED)), with samples loaded in a mixture with GelRed Nucleic Acid Stain (Biotium) and 10% glycerol. The native gel was run in 1× TBE buffer at 150V for 50 min. A BIO-RAD ChemiDoc MP Imaging system was used to scan the gel.

DNA adenine glycosylase (MYH) assay

FAM-labeled 32 nt-DNA molecules (40 nM) were incubated in reaction buffer of 20 mM Tris, pH 8.0, 1 mM ethylenediaminetetraacetic acid (EDTA), 1 mM Tris (2-carboxyethyl) phosphine (TCEP) and 0.1 mg/ml bovine serum albumin (BSA) at room temperature for 10 min. Addition of 200 nM DNA glycosylase (MYH) started the reaction. The reactions were incubated at room temperature for indicated time (up to 60 min) and quenched by addition of 0.1 M NaOH heating at 95°C for 10 min. Samples were mixed with 2× loading buffer (98% formamide, 1 mM EDTA and trace amount of bromophenol blue and xylene cyanole), and then heated at 95°C for 10 min and cooled on ice. A 5-μl sample was loaded onto a 10 cm × 10 cm denaturing PAGE gel containing 15% acrylamide, 7 M urea and 24% formamide in 1× TBE. The gel was run at 1X TBE buffer at 200 V for 35 min. A BIO-RAD ChemiDoc MP Imaging system was used to scan the gel. The intensities of the FAM-labeled product DNA were quantified and fitted via nonlinear regression: $[\text{Product}] = P_{max}(1-e^{-kt})$, where P_{max} is the product plateau level, k (min^{-1}) is the observed rate constant and t is the reaction time.

GST-pulldown assay

The protein fragments used are YTHDC1 residues 345–509 of UniProtKB/Swiss-Prot Q96MU7, YTHDC2 residues 1268–1430 of Q9H6S0, YTHDF1 residues 370–559 of Q9BYJ9 and YTHDF2 residues 391–579 of Q9Y5A9 and YTHDF3 residues 400–585 of Q7Z739. The YTH fragments as GST-tagged fusion in a pGEX-4T1 vector were synthesized by Biomatik. Each plasmid was transformed into BL21-CodonPlus cells for expression.

GST recombinant YTH domains were purified using glutathione sepharose beads (GE Healthcare). Biotinylated-methylated (N6mA) ssDNA, biotinylated-unmodified ssDNA, and untagged complementary short ssDNA oligonucleotides were synthesized through Integrated DNA Technologies. Biotinylated-ssDNA oligonucleotides, either methylated or unmodified, were annealed to the complementary short ssDNA oligonucleotide at a 1:3 ratio (10 mM Tris–HCl pH 7.5, 50 mM NaCl, 1 mM EDTA; 95°C for 5 min) to form dsDNA oligonucleotides. Pulldown assays were performed by pre-conjugating 5 μg of biotinylated-oligonucleotides, either ssDNA or dsDNA, to 25 μl of streptavidin agarose beads (Millipore) in binding buffer (20 mM Tris–HCl at pH 7.4, 200 mM KCl, 0.2 mM EDTA, 0.05% NP40) for 2 h at 4°C. Pre-conjugated beads were then incubated with 2 μg of GST-YTH domains in 500 μl of binding buffer for 2 h at 4°C. Pulldowns were washed three times with binding buffer and then beads were boiled in 30 μl of protein loading buffer. Pulldown samples were run on SDS-PAGE and Western blot analysis was conducted using GST antibody.

Crystallography

An Art Robbins Gryphon Crystallization Robot was used to set up screens of the sitting drop at ∼19°C via vapor diffusion method. The YTH domain YTHDC1 at a concentration of 12 mg/ml (∼0.6 mM) was incubated with DNA in a 1:2 molar ratio on ice for one hour. The 13-mer self-annealed oligonucleotide containing a central N6mA (5′-CAG-CTG-N6mA-GTC-GAC-3′) was dissolved in 10 mM Tris pH 7.5 and 50 mM NaCl to a 4 mM stock concentration. Crystals that grew in 10% (v/v) 2-propanol, 26% polyethylene glycol (PEG) 400, and 0.1 M sodium citrate tribasic dihydrate pH 5.0 gave rise to space group $P2_12_12_1$, whereas crystals that grew in 30% (v/v) 2-propanol, 0.1 M sodium citrate tribasic dihydrate and 0.1M sodium cacodylate pH 4.6 gave rise to space group $P3_221$ (Table 1).

Single crystals were flash frozen in liquid nitrogen by equilibrating in a cryoprotectant buffer containing the crystallization solution and 20% (v/v) ethylene glycol. X-ray diffraction data were collected at the SER-CAT beamline 22ID of the Advanced Photon Source at Argonne National Laboratory at wavelength of 1.0 Å. Crystallographic datasets were processed with HKL2000 (42). Molecular replacement was performed with the PHENIX PHASER module (43) by using the known structure of the human YTHDC1 YTH domain (PDB ID 4R3H) as a search model. Structure refinement was performed with PHENIX Refine (44), with 5% randomly chosen reflections for the validation by the R-free value. COOT (45) was used for the manual building of the structure and corrections between refinement rounds. DNA structures were built into difference electron densities during the first several rounds of refinement for the two complex structures. Structure quality was analyzed during PHENIX refinements and finally validated by the PDB validation server (46). Molecular graphics were generated by using PyMol (Schrödinger, LLC).

Table 1. Summary of X-ray data collection and refinement statistics (*)

Complex	YTH domain of YTHDC1	
DNA	5′-CAGCTGAGTCGAC-3′(A= N6mA)	
PDB code	7L4X	7L4Y
Date collected	2020–09-23	2020–09-23
Space group	$P3_221$	$P2_12_12_1$
Cell dimensions (Å)	56.74, 56.74, 108.96	45.97, 66.38, 77.61
α, β, γ (°)	90, 90, 120	90, 90, 90
Resolution (Å)	33.90–1.79 (1.85–1.79)	39.55–1.79 (1.85–1.79)
[a] R_{merge}	0.096 (0.934)	0.094 (0.794)
R_{pim}	0.024 (0.537)	0.027 (0.382)
$CC_{1/2}$, CC	(0.508, 0.821)	(0.738, 0.922)
[b] <I/σI>	17.5 (2.7)	21.6 (1.2)
Completeness (%)	99.8 (98.9)	86.5 (38.3)
Redundancy	17.5 (7.4)	11.1 (3.3)
Observed reflections	344,531	222,842
Unique reflections	19,738 (1934)	20,038 (872)
Refinement		
Resolution (Å)	1.79	1.79
No. reflections	19,701	19,974
[c] R_{work} / [d] R_{free}	0.182 / 0.223	0.202 / 0.235
No. atoms		
Protein	1312	1306
DNA	265	530
Solvent	111	92
B Factors (Å^2)		
Protein	42.1	36.8
DNA	54.3	46.8
Solvent	47.7	40.3
R.m.s. deviations		
Bond lengths (Å)	0.010	0.003
Bond angles (°)	1.0	0.6

*Values in parenthesis correspond to highest resolution shell.
[a] $R_{merge} = \Sigma|I - | / \Sigma I$, where I is the observed intensity and is the averaged intensity from multiple observations.
[b] <I/σI> = averaged ratio of the intensity (I) to the error of the intensity (σI).
[c] $R_{work} = \Sigma |F_{obs} - F_{call}| / \Sigma |F_{obs}|$, where F_{obs} and F_{cal} are the observed and calculated structure factors, respectively.
[d] R_{free} was calculated using a randomly chosen subset (5%) of the reflections not used in refinement.

RESULTS

MettL3-14 adenine methyltransferase complex is active on dsDNA containing cyclopyrimidine dimers

Because MettL3-14 is recruited to damaged sites within 2 min of UV irradiation (2), it is possible that methylation occurs before NER excision, and we asked whether MettL3-14 is active on dsDNA containing a cyclopyrimidine dimer (CPD), one of the major UV radiation-induced photoproducts (47). We synthesized a 28-bp DNA molecule, with a CPD flanked by at least eleven base pairs on either side, to assure the formation of one complete helical turn of dsDNA (Figure 1A). The complementary strand contains variations of the MettL3-14 target sequence (RRACH), as defined with RNA and DNA substrates (7,37). In addition, we included two controls: a dsDNA-containing five consecutive mismatched pairs (positive), and a fully paired duplex (negative). We first confirmed that MettL3-14 complex methylates the 28-nt ssDNA substrates about equally (Figure 1B and C). Lower but significant activity was observed on the 28-bp dsDNA-containing a CPD, as well as on the mismatched duplex, but MettL3-14 was completely inactive on the fully paired duplex (as expected). The level of activity on dsDNA containing a CPD was not affected by additional mismatched bases (comparing oligos 2, 3 and 4 to oligo 1), or by the excess of CPD-strand containing no recognition sequence—added to assure that the target strand is fully annealed (Figure 1D). The CPD may be sufficient to open a bubble in the dsDNA and expose the target A in a single-stranded region (Figure 1E) (48–50).

Under steady-state kinetic conditions, MettL3-14 methylates the 28-nt ssDNA with k_{cat} = 2.8 min^{-1} and K_m = 3.2 μM (Figure 1F). On the same DNA, but annealed with the complementary strand containing a CPD across from the RRACH motif, the MettL3-14 methylation rate is just ∼3-fold slower (k_{cat} = 0.9 min^{-1}) with ∼5-fold stronger binding affinity (K_m = 0.6–0.7 μM) (Figure 1G). In other words, MettL3-14 shows ∼1.5× higher catalytic efficiency of methylation on damaged dsDNA than on ssDNA (comparing k_{cat}/K_m value of ∼1.4 min^{-1} μM^{-1} for dsDNA and 0.9 min^{-1} μM^{-1} for ssDNA) (Figure 1H). Again, we note that MettL3-14 is essentially inactive on fully-base paired (undamaged) dsDNA. Thus damage- or mispairing-induced bubbles in dsDNA substantially enhance adenine methylation at those sites.

MettL3-14 complex is active on dsDNA containing CPD hotspots

We next considered whether MettL3-14 can act on promoters containing CPD hotspots—associated with UV-exposed cancer risks—basing our analysis on previous results from others. Two groups used a CPD-seq method (51) to map the distribution of UV-induced CPD lesions across the human genome, where DNA was harvested immediately following UV-irradiation (and thus before DNA repair), and CPD sites were specifically cleaved and could be targeted by ligation. These studies found that CPD lesions are elevated at transcription factor binding sites, particularly at E26 transformation-specific (ETS) binding sites (52,53). There are two major CPD peaks associated with active ETS binding sites (TTCCG): the first is within the ETS binding sequence and forms between the two internal consecutive pyrimidine bases TC (T**TC**CG) and CC (TT**CC**G), while the second is between two bases immediately 5′ of the TTCCG element if both bases happen to be pyrimidines (**TC**TTCCG). This enrichment of CPD lesions correlates with elevated mutation rates, primarily C-to-T, that drive recurrent mutagenesis in melanomas. One example is the highly mutated ETS binding sites in the promoter of *RPL13A* (ribosomal protein L13A), where the recurrent C-to-T mutations of T**C**TT**C**CG are seen in this most-frequently mutated ETS element in the melanoma dataset of the International Cancer Genome Consortium (54). We note that between the thymine and cytosine that form a CPD, it is a C-to-T transition that primarily occurs in UV-induced mutations, and there is essentially little to no mutation involving the thymine. This is consistent with the observations that mutation is not enhanced in the first two pyrimidines in the ETS site (**TT**CCG), and that the most common mutational signatures of UV irradiation are T**C**G→TTG and T**C**C→TTC (55). Interestingly, two highly recurrent, cancer specific C-to-T mutations in the TC

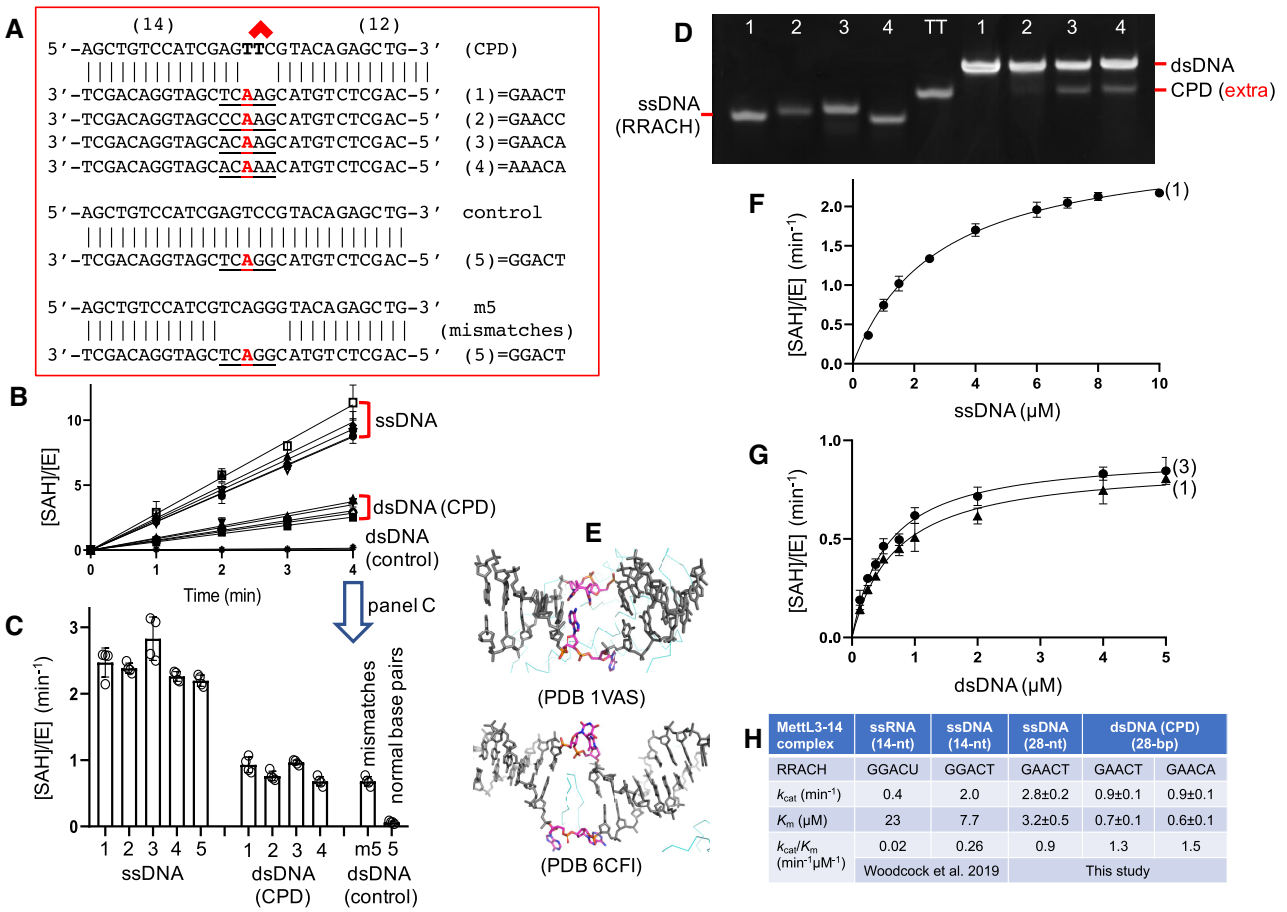

H

MettL3-14 complex	ssRNA (14-nt)	ssDNA (14-nt)	ssDNA (28-nt)	dsDNA (CPD) (28-bp)	
RRACH	GGACU	GGACT	GAACT	GAACT	GAACA
k_{cat} (min^{-1})	0.4	2.0	2.8±0.2	0.9±0.1	0.9±0.1
K_m (μM)	23	7.7	3.2±0.5	0.7±0.1	0.6±0.1
k_{cat}/K_m (min^{-1}μM^{-1})	0.02	0.26	0.9	1.3	1.5
	Woodcock et al. 2019		This study		

Figure 1. MettL3-14 is active on CPD-containing dsDNA. (**A**) DNA oligos used in this experiment. The target consensus sequences of MettL3-14 are underlined (RRACH; where R = puRine, and H = not G). (**B**, **C**) Under the same laboratory conditions, MettL3-14 is active on ssDNA, dsDNA containing CPD or mismatches, but is inactive on a fully paired duplex (control). (**D**) A 15% native gel showing RRACH-containing ssDNA and dsDNA with a complementary CPD-containing strand (which contains no recognition sequence). Note that an excess of CPD-strand was used in annealing with oligos #3 and #4. (**E**) The DNA structures containing a CPD bound to T4 endonuclease V (PDB 1VAS) or a 6–4 photoproduct bound to Rad4-Rad23 (PDB 6CFI). (**F**) MettL3-14 activity on ssDNA (oligo #1). (**G**) MettL3-14 activity on dsDNA (oligo #3 or #1 paired with the CPD strand), with varying concentrations of substrate DNA. (**H**) Summary of kinetic parameters of MettL3-14. Increased ssDNA size from 14-nt to 28-nt resulted in slightly increased k_{cat} (1.4×) and ∼2.4× enhanced binding affinity (K_m value from 7.7 to 3.2 μM). Data represent the mean ± SD of two independent determinations, with duplicates assayed for each of the two determinations.

dinucleotides in the promoter of *TERT* (telomerase reverse transcriptase) (56–61), created an identical 11-bp sequence [5′-CCCCT(C→T)CCGGG-3′] that contains an ETS binding site (TTCCG). Similar creation of a new ETS binding site within this promoter is also associated with thyroid carcinoma (62), glioblastoma (63), meningioma (64), and hepatocellular carcinoma (65). While these other cancers are unlikely to result directly from UV exposure, we note that it is possible to generate CPDs without the direct contribution of UV radiation (66–68).

Based on the preceding, we first asked whether the CPD-containing promoter sequence of *RPL13A* is a substrate of MettL3-14. The mutation hotspot of *RPL13A* contains six pyrimidines (TCTTCC), and the complimentary strand contains six purines, which partially matches the degenerate MettL3-14 substrate sequence RRACH (G**GAAG**A) (Figure 2A). We previously showed that MettL3-14 has measurable but low activity on a short ssDNA containing GGA**G**T in place of GGA**C**T (37). First, we thus repeated the experiment on ssDNA containing the purine strand of the *RPL13A* promoter sequence (GAA**G**A) and its G-to-C substitution (GAA**C**A) to match the RRACH consensus (Figure 2B). This showed that GAA**G**A (oligo #2; k_{obs} = 0.15 min^{-1}) yields ∼5× lower activity than the GAA**C**A (oligo #3; k_{obs} = 0.8 min^{-1}), and further ∼2× lower activity than the GGA**C**A (oligo #1; k_{obs} = 1.5 min^{-1}). We note that oligo #1 has an additional GGA**C**C sequence located at the 3′ end. The methylation activity on GAA**G**A is enzyme concentration dependent, as the activity increases with the enzyme concentration (Figure 2C).

Second, as expected, we confirmed that MettL3-14 is inactive on fully-paired dsDNA representing this promoter (annealed oligos 1+2 in Figure 2D), even though the pyrimidine strand (oligo #1) has the highest activity on its single-stranded form (Figure 2E). However, MettL3-14 has weak but measurable activity on dsDNA containing just one mismatch (C:C) immediately 3′ to the target adenine (annealed oligos 1+3 in Figure 2D and E).

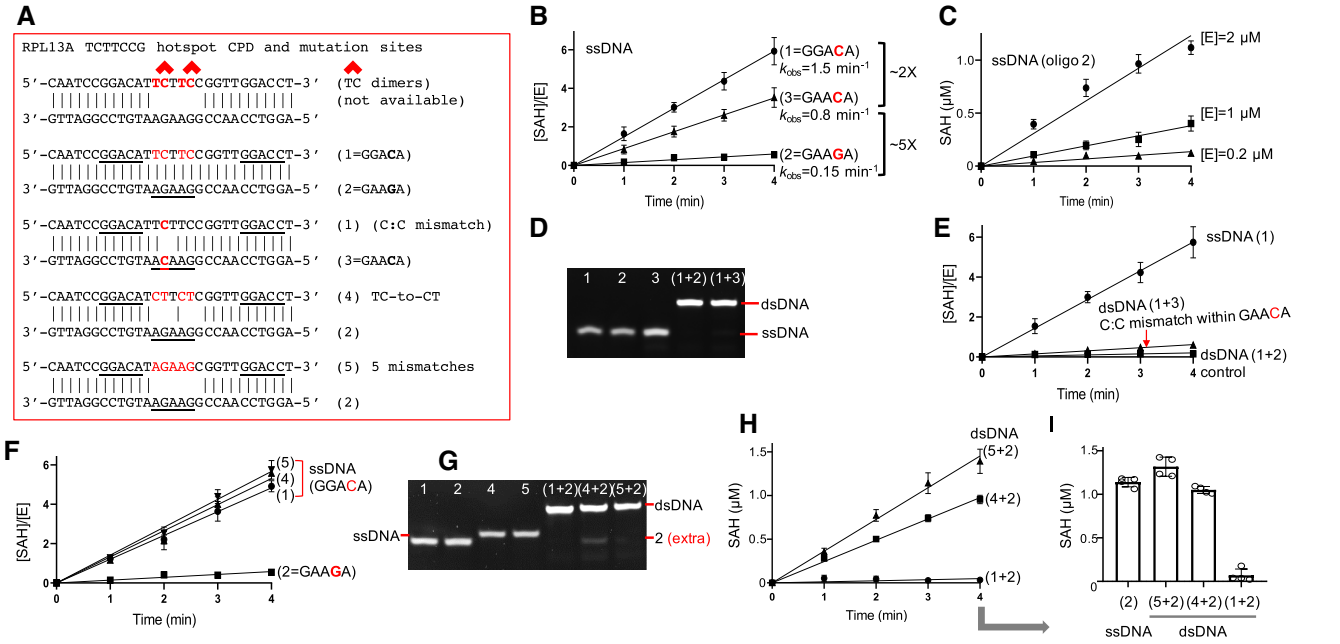

Figure 2. MettL3-14 is active on GGAGA sequence. (**A**) DNA oligos used in this experiment. The sequence is taken from the recurrent C-to-T mutations in the promoter of *RPL13A*. "Not available" refers to commercial phosphoramidites of TpC dimer for use in DNA synthesis. (**B**) Under the same laboratory conditions, MettL3-14 is active on ssDNA containing GGACA (#1), GAACA (#3) and GGAGA (#2). (**C**) Methylation activity on ssDNA containing GGAGA (#2) increases as enzyme MettL3-14 concentration increases. (**D**) A 15% native gel showing ssDNA and dsDNA containing mismatches as defined in panel A. (**E**) MettL3-14 has weak activity on dsDNA containing one mismatch immediately next to the target adenine. (**F**) Comparison of MettL3-14 activity on ssDNA containing GGA**C**A (oligos #1, #4 and #5) or GAA**G**A (#2). (**G**) A 15% native gel showing ssDNA and dsDNA containing mismatches. Note that excess ssDNA oligo #2 was used in annealing with oligo #4. (**H**, **I**) MettL3-14 is active on mismatched dsDNA containing GGA**G**A.

Third, we looked more carefully at duplexes containing mismatches, in part because there are no commercially-available phosphoramidites of TpC dimer for use in DNA synthesis (per Biosynthesis); and due to a prolonged delay in DNA synthesis, during COVID-19 pandemic, of substituting the two TC dimers with TT dimers in the *RPL13A* promoter sequence. Accordingly, we designed mismatched oligos either in the places of two TC dimers (oligo #4 in Figure 2A) or five consecutive mismatches covering the MettL3-14 substrate site (**GAAGA**) (oligo #5 in Figure 2A). We reasoned that the methylation activities on dsDNA containing either one CPD or five mismatches are comparable (Figure 1C), as the mismatches may facilitate strand separation in the dsDNA and could be used to mimic the two TC dimers in the promoter of *RPL13A*. We first confirmed that ssDNA of oligos #4, #5 and #1 have equivalent activity (all three contain GGA**C**A) (Figure 2F). The dsDNA generated by annealing oligos #4 or #5 respectively to oligo #2 resulted in four or five mismatches covering the **GAAGA** site (Figure 2A). Because the ssDNA of oligos #4 and #5 (GGA**C**A) each yield higher activity than oligo #2 (GAA**G**A), we used excess of oligo 2 in the annealing procedure to assure that the oligo #4 is fully annealed (Figure 2G). The level of activity of MettL3-14 on dsDNA containing the four or five mismatches are approximately the same (dsDNA 4+2 and 5+2 in Figure 2H), and the activity is similar to that of ssDNA containing GAA**G**A (Figure 2I).

Together, these results indicate that the GAAGA sequence, opposite to the two TC dimers in TCTTC mutation hotspots, could be methylated by MettL3-14 *in vitro* in the context of damage, though the methylation activity was weaker when the adenine was followed by a guanine (ApG) than by a cytosine (ApC). Furthermore, if the damaged site is accessible and the enzyme-mediated strand separation (Figure 1E and ref. (69)) is large enough, the adenine residues in the purine-rich sequence could all be methylated (GGAAGAAT) if the sequence preference for AC (in the RRACH consensus) is relaxed.

MettL3-14 complex is active on dsDNA containing an A across from an abasic site

In addition to CPD, abasic sites (missing a nucleobase but with the sugar-phosphate backbone intact) are another frequent DNA lesion—formed as a result of DNA damage and a key intermediate during the base excision repair. Abasic sites can lead to mutations and strand breaks (reviewed in (70) and references therein). In the genome of (human-derived) HeLa cells, some abasic sites persist long enough to be detected at single-base resolution, even in the presence of apurinic/apyrimidinic endonuclease 1 (APE1) (71), which is the main endonuclease to initiate repair at abasic sites in mammalian cells (72). Here, we asked whether dsDNA containing an abasic site opposite to adenine is a substrate of MettL3-14. We designed duplexes with one or two abasic sites opposite to AA or GA (Figure 3A and B). MettL3-14 has comparable activity on abasic-containing dsDNA to that of mismatches and CPD-containing oligos (Figure 3C–E).

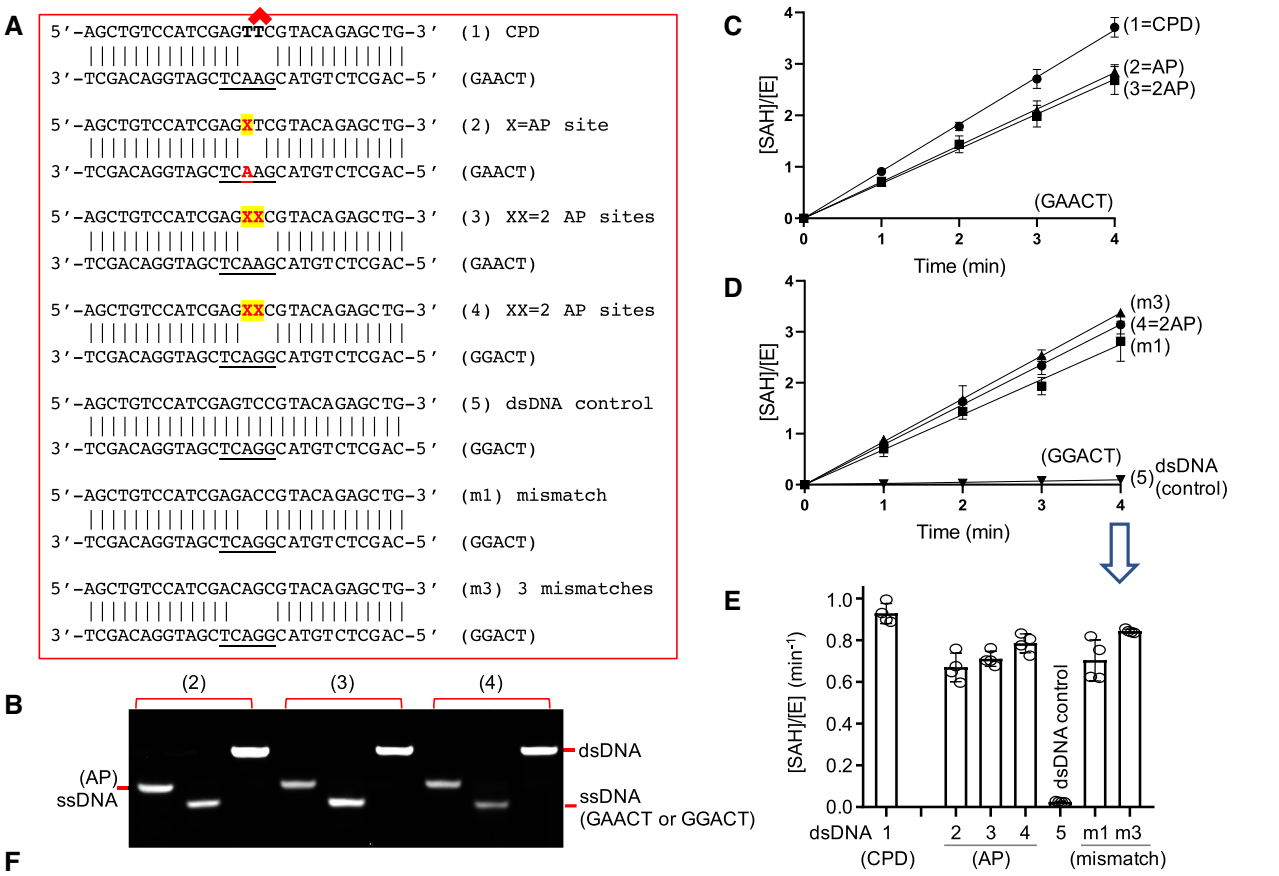

F

MettL3-14 complex	dsDNA (28-bp)									
	CPD		2 AP sites		mismatches (underlined)					
DNA	GAACT	GAACA	GAACT	GGACT	GAACT	GAACT	GAACT	GAACA	GAAGA	GAAGA
k_{obs} (min^{-1})	0.9±0.1	0.9±0.1	0.71±0.02	0.78±0.02	0.68±0.04	0.81±0.03	0.78±0.04	0.23±0.01	0.16±0.03	0.16±0.03

Figure 3. MettL3-14 is active on dsDNA containing abasic (AP) sites. (**A**) DNA oligos used in this experiment (X = AP site). (**B**) A 15% native gel showing AP-containing ssDNA and dsDNA with a complementary strand containing either GAACT (oligos #2 and #3) or GGACT (oligo #4). (**C**) Under the same laboratory conditions, MettL3-14 is active on dsDNA containing CPD or AP sites. Oligos #1, #2 and #3 are paired with GAACT. (**D**) MettL3-14 is active on dsDNA containing mismatches, but is inactive on a fully paired duplex (control). Oligos #4, #5, m1 and m3 are paired with GGACT. (**E**) Activities of MettL3-14 at 4 min for different substrates. Data represent the mean ± SD of two independent determinations, with duplicates assayed for each of the two determinations. (**F**) Summary of activities of MettL3-14 on damaged dsDNA examined in this study.

To summarize our analyses, we compared MettL3-14 methylation activities on all dsDNA substrates examined in this study (Figure 3F). The apparent k_{obs} values are relatively similar (0.7–0.9 min^{-1}) on damaged dsDNA, whether the damage involves CPDs, abasic sites, or mismatches centered on the target adenine. If the mismatch moves away from the target adenine, but is still within the 5-nt recognition sequence, the activity is reduced by ∼3× (comparing GAACA versus GAACT with underlined base in mismatch). Similarly, the activity is reduced by ∼5×, but measurable, with substitution of guanine in the place of cytosine (comparing GAAGA versus GAACA).

DNA adenine methylation inhibits base excision of adenine by MutY glycosylase homolog

After removing a short stretch of ssDNA containing a lesion, repair-associated DNA synthesis requires DNA polymerases for gap-filling synthesis. DNA polymerases, including error-prone polymerases, are important for NER repair synthesis in human cells (73). As noted above, between the thymine and cytosine residues forming CPD lesions, thymine is not typically mutated, and instead there are predominantly C-to-T substitutions. The underlying mechanism of elevated C-to-T mutation densities, at the CPD lesions of ETS-related promoter, is currently unknown. Mao *et al.* and Elliott *et al.* ruled out inhibited NER repair activity due to ETS1 binding as a major cause of elevated somatic mutation rates (52,53). One potential possibility is that some low-fidelity DNA polymerases (pol η and pol ν) are more prone to dT misincorporation opposite template G, and thus promote C-to-T hypermutation in somatic cells (74–76).

Similarly some DNA polymerases have a higher tendency to misincorporate free 8-oxo-dGTP, from the deoxynucleotide triphosphate pool (77), into DNA opposite

template adenosines, using Hoogsteen pairing (78–81). It was suggested that N6mA in mammalian DNA can reduce misincorporation of 8-oxoG opposite to A by DNA polymerases (82). However, once incorporated into DNA, there is no known repair activity that removes 8-oxoG opposite to template A. The mammalian mismatch repair system has been proposed to provide an independent supplementary layer of protection, via an OGG1-like glycosylase activity, by excising 8-oxoG opposite to C following incorporation from the dNTP pool (83). In *Saccharomyces cerevisiae* the mismatch repair complex, via a MutY-like glycosylase activity, removes A paired with 8-oxoG (84). This is a double-edged sword, however. Mammalian MutY glycosylase homolog (MYH) does correctly repair 8-oxoG:A pairs resulting from misincorporation of A across from 8-oxoG (85). However in the reverse case of misincorporation of 8-oxoG across from the (correct) A, this A removal 'locks in' a T-to-G transversion (Figure 4A), as shown with E. coli MutY (86). Clearly, the mispairing of 8-oxoG with A poses an unacceptable mutation risk.

We examined the effect of N6mA on mammalian MYH. We measured the base excision activity of MYH using 32-bp DNA oligos, each containing one of the following single mismatches: 8-oxoG:A, G:A, 8-oxoG:N6mA or G:N6mA (Figure 4B). As expected, MYH cleaves the adenine opposite 8-oxoG with an apparent $k_{obs} = 2.8\ min^{-1}$ under single-turnover conditions (Figure 4C). MYH also excises A from G:A mispairs (87), though with an ∼30-fold lower catalytic rate ($k_{obs} < 0.1\ min^{-1}$). Adenine methylation changes this substantially. To begin with, no MYH activity at all was detectable on G:N6mA. When the excision reaction is nearly complete for a 8-oxoxG:A mispair, at 2-min reaction time, the reaction on 8-oxoG:N6mA is barely measurable (Figure 4D). Put another way, the A excision activity on 8-oxoG:N6mA is more than 70X slower than on 8-oxoG:A ($k_{obs} < 0.04\ min^{-1}$).

In summary, the relative MYH excision rates were 8-oxoG:A (1X) > G:A (reduced ∼30X) >> 8-oxoG:N6mA (reduced >70X) >>>> G:N6mA (unmeasurable). This suggests that, if 8-oxoG does pair with template N6mA in dsDNA, the methylation interferes with repair and is thus promutagenic. However, this effect is countered by the reduced pairing of 8-oxoG with N6mA (compared to unmethylated A) by DNA polymerases (82,88). To compare these competing effects to 8-oxoG:A pairs, 8-oxoG:N6mA pairs are ∼70X less likely to be repaired (this study), but ∼10X less likely to form in the first place (82).

YTH domain of YTHDC1 binds N6-methyladenine located across from a single base gap between two canonical DNA helices

Homologous recombination-mediated repair involves several distinct pathways that generate intermediates with ssDNA regions, non-B DNA D-loop structures, or four-way Holliday junctions ((8) and references therein). Thus consideration of a role for N6mA in modulating mutation rates could depend on whether N6mA is recognized in these altered structural contexts. YTH domain-containing proteins have been studied extensively for their ability to bind N6mA-containing RNA in mammalian cells (89). Interestingly, YTHDC1 is recruited to DNA DSBs (3), and binds to ssDNA containing N6mA *in vitro* (40). Under the same conditions, the YTH domain of YTHDC1 binds N6mA in a DNA context with an affinity stronger by a factor of five than such binding in an RNA context (40). A recent study in human sarcoma U2OS cells suggests that a MettL3-N6mA-YTHDC1 pathway modulates homologous recombination-mediated repair (3) which, as noted above, involves non-B DNA conformations. In previous studies, we have not observed binding of the YTH domain of YTHDC1 to fully-paired (ds)DNA or to fully-paired RNA/DNA hybrid oligos that included N6mA on one strand (40). Here we demonstrate that the YTH domain of YTHDC1 recognizes N6mA located across from a single base gap and linking two perpendicular DNA helices.

We designed a 13-nt oligonucleotide with the central N6mA flanked by six nucleotides on either side. The oligonucleotide is self-annealed, forming an extended gapped duplex, with single N6mA nucleotides on one strand connecting two six-bp DNA duplexes (Figure 5A). We co-crystallized the YTH domain of YTHDC1, complexed with the N6mA-containing DNA, in the two space groups of $P2_12_12_1$ and $P3_221$ (Figure 5B-C). In the space group $P2_12_12_1$, only half of the N6mA sites are bound by YTH, whereas in $P3_221$, every N6mA is bound. The two DNA-bound YTH complexes, though in different space groups, are highly similar, with a root-mean-square deviation of 0.185 Å over 137 pairs of residues. Comparing the DNA components within the space group $P2_12_12_1$, with and without YTH binding, the N6mA stacks against the 5′ side of guanine in the absence of YTH (Figure 5D), whereas this N6mA moves away from the 5′ G (Figure 5E) and is inserted into the aromatic binding pocket of the YTH domain when present (Figure 5F), as was observed for complexes with ssRNA and ssDNA (40,90). The N6mA-binding pocket is highly conserved among vertebrate YTH family orthologs, including the sidechain (Trp428) that contacts the N6mA methyl group (40).

Structural superimposition of YTH-dsDNA, onto YTH-ssRNA and YTH-ssDNA, revealed that the conserved interactions involve the nucleotides immediately 3′ to the target N6mA (= A; Figure 5G). The 3′ AGT of dsDNA is superimposable with the corresponding ACU of the RNA and ACT of ssDNA. In all three instances the three phosphate groups 3′ to the target N6mA (labeled as P1, P2 and P3 in Figure 5H) are bound at the basic surface track of YTH (Figure 5I).

There are also three interactions unique to the dsDNA recognition. First, Leu380 and Pro381 provide van der Waals contacts to the G:C base pair immediately 5′ to N6mA (Figure 5J), from which Leu380 would replace the N6mA that stacks with the 5′ G in the unbound state (see Figure 5D). We note that these interactions are not base specific—other than the target N6mA itself there are no base-specific interactions (Figure 5F). The second dsDNA-specific interactions involve Arg475 and Ser435, which contact phosphates on opposite strands (Figure 5K). Arg475 H-bonds with three phosphates, two 5′ and one 3′ to the target N6mA. Third, and finally, two lysine residues, Lys437 and Lys469, probably participate in interactions (respectively) with the phosphate groups at the two ends of the non-

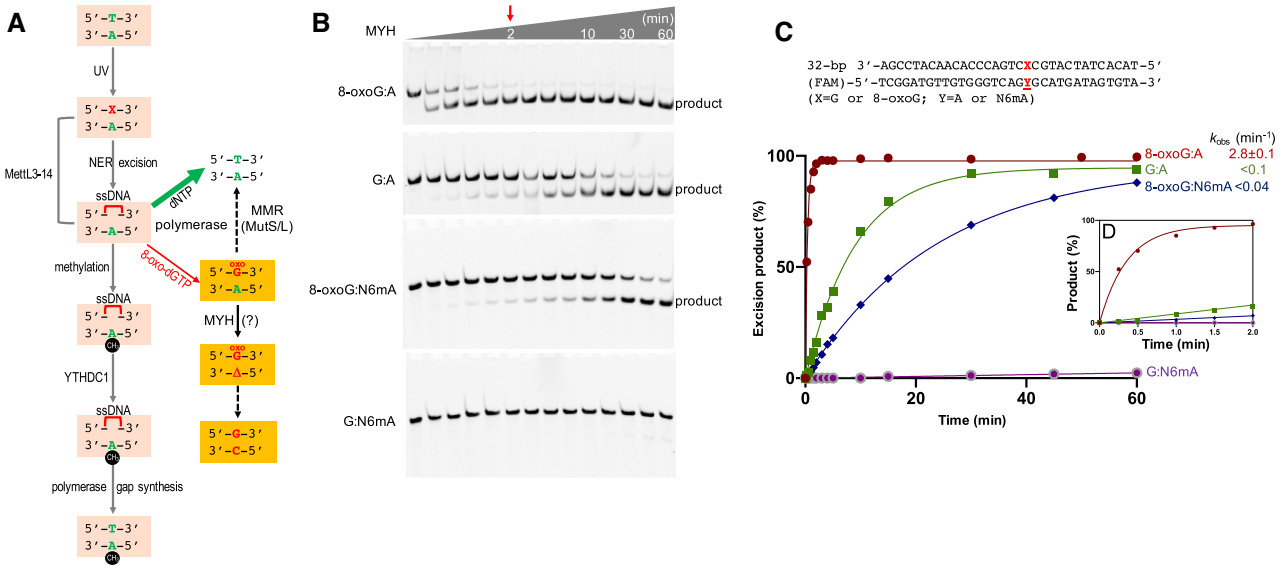

Figure 4. N6mA inhibits base excision of adenine by MYH glycosylase. (**A**) A model for how N6mA could reduce the rate of T-to-G mutation by reducing misincorporation of 8-oxoG opposite to Ade. Adenine methylation could occur either before or after excision, in the lesion-containing dsDNA (marked with the red X) or in the transiently-generated ssDNA gap (∼25–30 nt; the red bracket). DNA synthesis would be largely accurate because T is preferentially inserted opposite A (bold green arrow). However, reactive oxygen species can lead to the formation of 8-oxo-dGTP in the dNTP pool and, in the event that 8-oxo-dGTP is incorporated into DNA during synthesis, it may be mispaired opposite adenine (Ade) (red arrow). In the latter event, mismatch repair (MMR) most likely excises incorporated 8-oxo-2′-deoxyguanosine (8-oxoG) from newly synthesized daughter DNA (dashed line) or base excision of the (correct) Ade by the MYH DNA adenine glycosylase, and can result in a T-to-G transversion mutation (orange boxes). Recruitment of YTHDC1 protects N6mA-containing DNA. (**B**) The glycosylase activity of MYH as a function of time on dsDNA substrates containing all four mismatch combinations of X:Y (X = 8-oxoG or G, and Y = A or N6mA). The oligonucleotide was labeled with FAM on the bottom (Y) strand. The products of the reactions were separated on a denaturing polyacrylamide gel, and the FAM-labeled strand was excited by UV and photographed. (**C**) The intensities of the FAM-labeled DNA were quantified and fitted via nonlinear regression. (**D**, inset) The products made within the first 2 min. The adenine excision is nearly completed for the 8-oxoG:A mispair, while the reaction involving 8-oxoG:N6mA is barely measurable.

target strand (currently not included in the DNA synthesis) (Figure 5L).

These dsDNA-specific interactions are shared by both dsDNA oligos, which are held by multiple points of attachment to both strands, constraining their relative orientation in the YTH-dsDNA complex. Finally, the conformations of the two nucleotides 5′ to N6mA, that were observed in RNA (90), cannot be accommodated in dsDNA as they would be incompatible with the duplex (Figure 5M).

In the YTHDC1-dsDNA structure, eight residues were found to contact the flipped-out N6mA base (blue in Figure 6A), and 15 more residues made other DNA contacts (red in Figure 6A). We note that some of these dsDNA-contacting residues are conserved, not only among vertebrate YTHDC1 orthologs, but also among YTHDF1-3 orthologs (40). Of the N6mA-contacting set, only N363 is unique to YTHDC1; N367 is also present in YTHDC2, while the other six are present in all five proteins, though S378/T379 is substituted conservatively by CS in the three YTHDF proteins.

For the 15 other DNA-interacting residues, six are unique to YTHDC1 (L380, E405, M434, M438, K472 and G474), two are shared only with YTHDC2 (P381, L439) (Figure 6A), and four are universally shared (K361, N466, K469, R475). The dsDNA-specific contacts Leu380 and Pro381 (LP) are not conserved, and are substituted by TP in YTHDC2 or TE in YTHDF1–3 (Figure 6A). Ser435 and Lys437 are located in a loop region of varying length. Ser435 is an Asn in most vertebrate YTHDC1 orthologs [see Supplementary Table S2 in (40)], and the (S/N)AK in YTHDC1 is absent in YTHDC2, but could be replaced by the spatially-equivalent residues SQDK in YTHDF1–3 (Figure 6A). This conservation raises the possibility that other members of the YTH family might bind some forms of dsDNA as well, even though YTHDC1 and DC2 are unrelated to each other and only distantly related to YTHDF1–3, based on amino acid sequence, size, and overall domain organization (89). Interestingly, a GST-pulldown experiment indicated all five YTH domains are capable of binding ssDNA containing N6mA. Four of them, all except for YTHDC2, also bind nicked dsDNA (Figure 6B). YTHDC2 has a number of residues that are unique among this set of proteins (yellow highlighting in Figure 6A), and its uniqueness in not binding the nicked DNA substrate is reminiscent of its difference from the other four YTH domains in binding certain RNA adenine modifications (91).

While the 6-bp duplex on each side of N6mA adopts a B-form helix, the axes of the two duplexes bound to one YTH domain are virtually perpendicular to one another (Figure 7A). To our surprise, the YTH-bound DNA molecule—from two adjacent duplexes at a ∼90° angle—is strikingly similar to both the nicked DNA produced by cleavage of a four-way Holliday junction by the resolving nuclease GEN1 from *C. thermophilum* (Figure 7B) (92), and to dsDNA nicked by human FEN1 Flap endonuclease (Figure 7C) (93). Both FEN1 and GEN1 are members of the nuclease family acting in nucleotide excision repair,

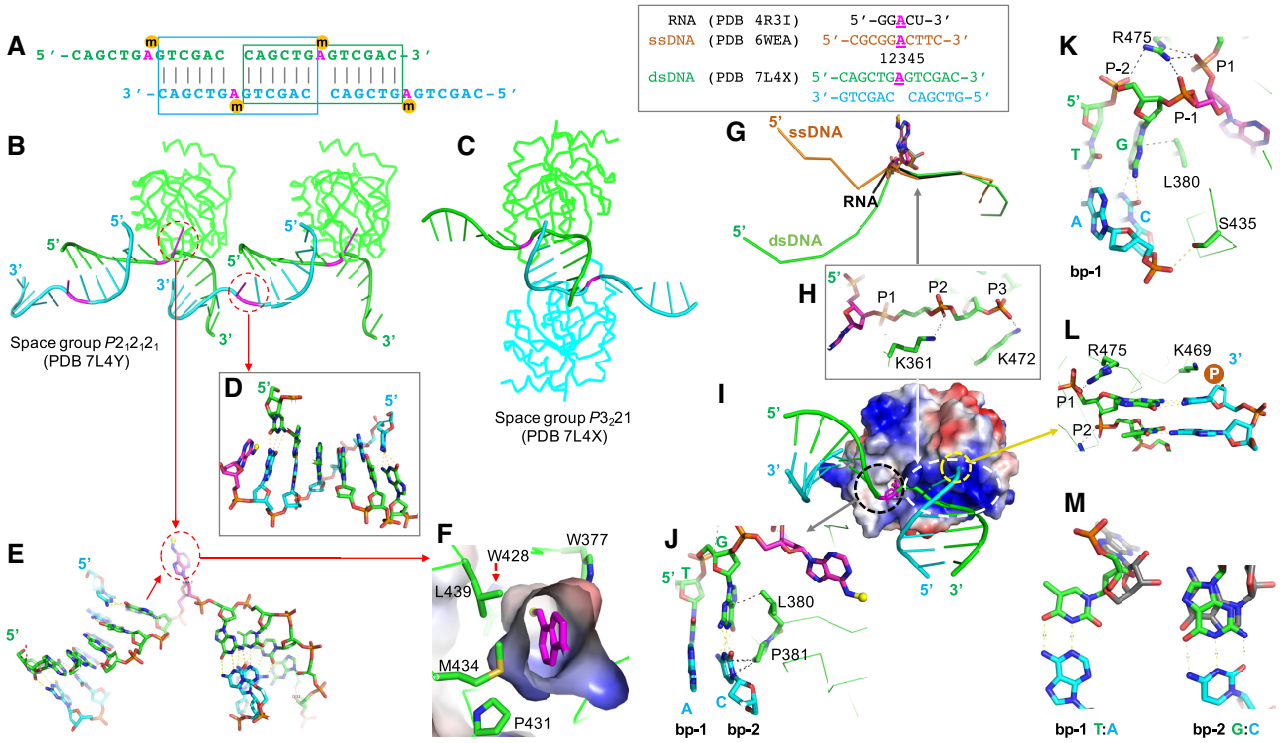

Figure 5. Structure of YTH domain of YTHDC1 bound to dsDNA containing a gap. (**A**) DNA oligo designed for co-crystallization with YTH. (**B**, **C**) The YTH-dsDNA complexes crystallized in two different space groups. (**D**) The unbound N6mA stacks with 5′ Gua. (**E**) The YTH-bound N6mA is no longer stacked with the 5′ DNA base. (**F**) YTH domain contains a hydrophobic pocket for binding N6mA. (**G**) Superimposition of YTH domain of YTHDC1 in complex with RNA, ssDNA and dsDNA. For simplicity, only the target strand is shown (colored in green); i.e. the dsDNA strand containing the N6mA. Base pair (bp) positions are numbered as 1–5. (**H**) Three phosphate groups 3′ to N6mA (P1, P2 and P3) have conserved interactions with YTH. (**I**) YTH domain contains a basic surface (circled with a dashed line) next to the N6mA-binding. (**J**) Leu380-Pro381 dipeptide forms stacking interaction with G:C base pair at bp position 2. (**K**) Arg475 bridges among three phosphate groups of the target strand, and Ser435 interacts with the phosphate group between bp positions 1 and 2 of the non-target strand. (**L**) A potential interaction with 3′ phosphate group of nucleotide at position 4 of the non-target strand by Lys469, which is fully conserved in all three YTH families (40). (**M**) Superimposition of YTH-bound RNA strand (in grey) and dsDNA (in color) at bp positions 1 and 2.

mismatch repair and homologous recombination; and incise structurally distinct bubbles, ends or Holliday junctions (94). Thus YTH (at least) recognizes N6mA specifically in a structural context associated with mutation repair.

DISCUSSION

A role for N6mA in DNA damage repair

The writer and reader of N6mA, MettL3-14 and YTHDC1 respectively, both have been enriched at the damaged sites and implicated in modulating nucleotide-excision repair and homologous recombination-mediated repair (2,3). Using *in vitro* biochemical approaches, we show that MettL3-14 and YTHDC1 are active on ssDNA and lesion-containing dsDNA. This led to the hypothesis that damage-induced generation of N6mA in DNA reduces misincorporation of 8-oxoG opposite to Ade that, if not repaired in time, would yield T-to-G mutations (Figure 4A), which is rare in the case of mutation resulting from thymine involved in CPD formation.

UV damage results in bulky DNA adducts; these adducts are mostly CPD and 6,4-photoproducts, opposite to the complementary ApA, ApG or GpA dinucleotides. Recognition of this damage by xeroderma pigmentosum C protein (95) leads to subsequent excision and removal of a segment of ssDNA that contains the lesion, resulting in single-stranded regions in the genome. Rapid recruitment of MettL3-14 to the damaged sites could mean that adenine methylation occurs either before excision or in the transiently-generated ssDNA, followed by the recruitment of YTHDC1 to N6mA-containing DNA (Figure 4A). The specificity of YTHDC1 affinity for nicked, as well as N6mA-containing, DNA is illustrated by our observation that family member YTHDC2 has lost the former but retains the latter (Figure 6B). The YTHDC1 might protect against, for example, demethylation by ALKBH1, which (like MettL3-14) also acts on damaged or unpaired DNA (96). The undamaged, adenine-methylated ssDNA template would assist the error-prone DNA polymerases in synthesizing the short complementary sequence by substantially reducing the misincorporation of 8-oxoG opposite to N6mA (82). When 8-oxoG nevertheless is misincorporated opposite N6mA, the methylation inhibits removal, by either MYH or the mismatch repair system, of the N6mA from the (presumptively correct) template strand (Figure 4B).

For comparison, *E. coli* uses N6mA to identify the parental DNA strand during mismatch repair (97), though in that case the N6mA directs from which strand a segment

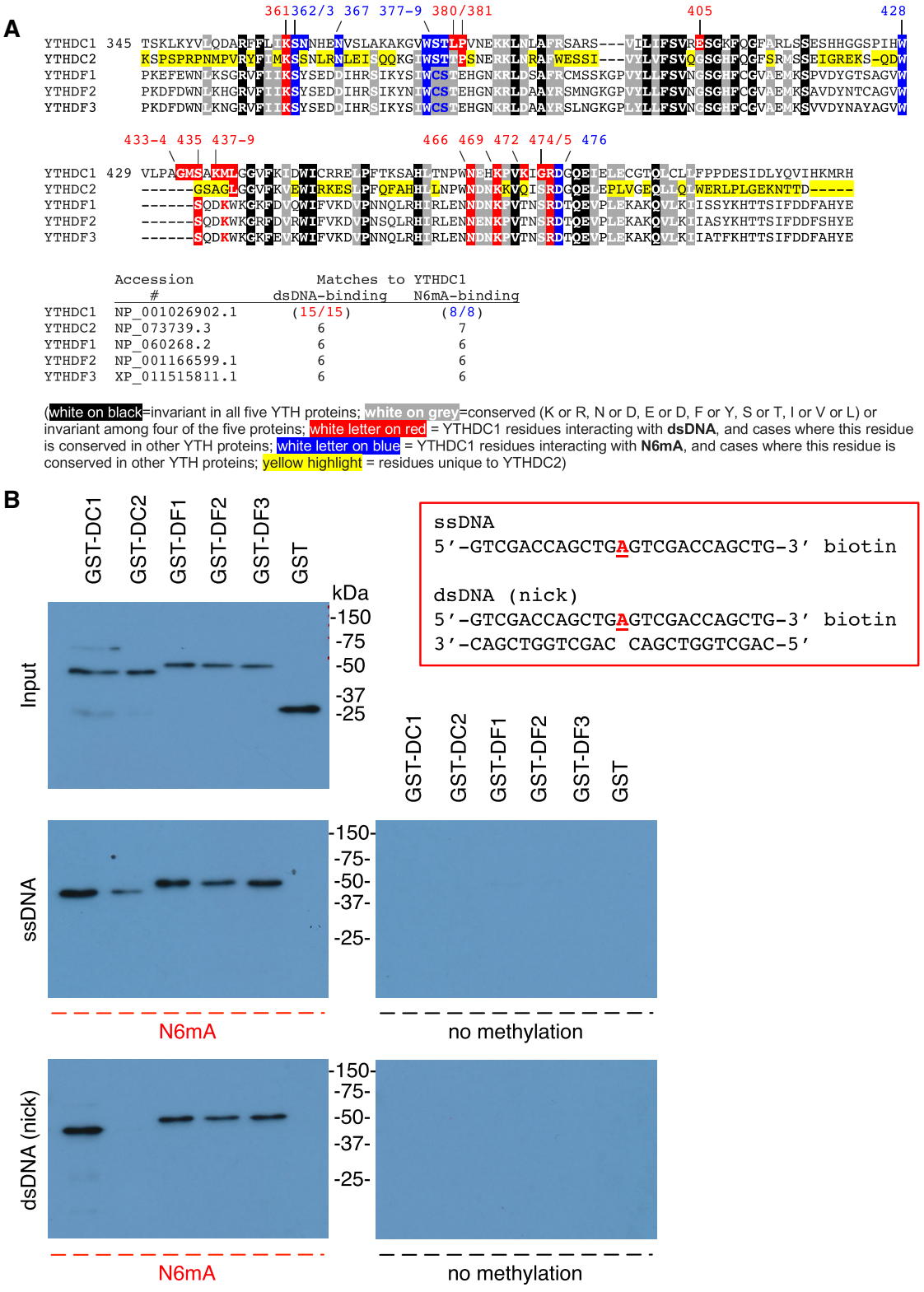

Figure 6. Five human YTH domain proteins. (**A**) Sequence comparison of five YTH domains. As described in the panel, residues of YTHDC1 that interact with N6mA or other DNA elements are numbered and highlighted, along with matches at equivalent positions in the other proteins. The number of relevant positions that match those in YTHDC1 are indicated, and include as 'matching' a lysine in the three YTHDF proteins that is one position over from K437. (**B**) DNA oligos used in the GST pulldown experiment, with underlined A either methylated (N6mA) or unmodified. All five YTH domains are capable of binding ssDNA containing N6mA. Four of them, all except for YTHDC2, also bind nicked dsDNA containing N6mA.

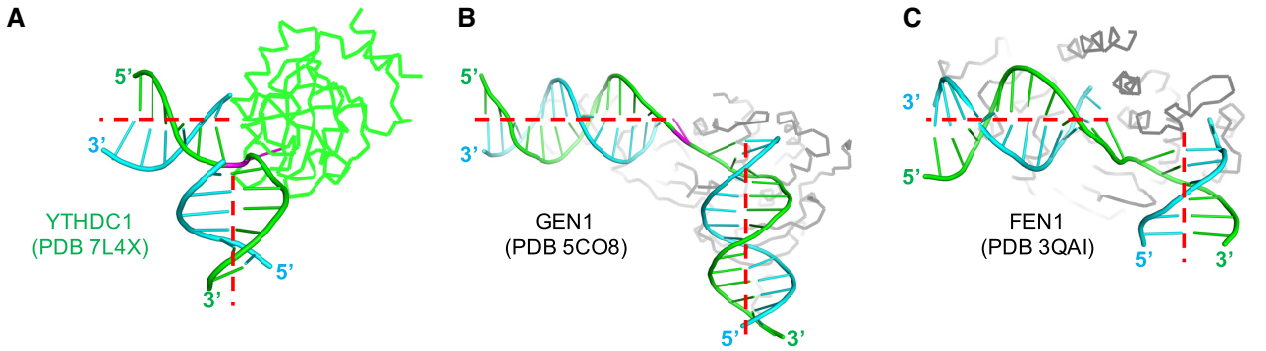

Figure 7. Similar DNA conformations seen in DNA complexes with YTH (**A**), GEN1 (**B**), and FEN1 (**C**). Two nearly perpendicularly-arranged DNA duplexes are linked by a gap nucleotide (i.e. one continuous strand in green, and one strand in cyan with a missing nucleotide or backbone cleavage).

should be removed and replaced. In the model proposed here, the N6mA is not only a signal to recruit proteins, but is an intrinsically protective modification at potential mutation hotspots. In light of our *in vitro* observations, further *in vivo* experiments to monitor the consequence of DNA adenine methylation during the DNA repair processes might provide a trackable biological system to follow the establishment, recognition and erasure of N6mA in DNA.

DATA AVAILABILITY

The YTH domain of YTHDC1 X-ray structures (coordinates and structure factor files) have been submitted to PDB under accession numbers 7L4X (YTHDC1-N6mA in $P3_221$) and 7L4Y (YTHDC1-N6mA in $P2_12_12_1$).

ACKNOWLEDGEMENTS

We thank Dr Tao Wu at Baylor College of Medicine for discussions and Ms Yu Cao for technical assistance. We thank Dr Clayton B. Woodcock and Dr Samuel Hong for their previous involvement in protein purifications of YTHDC1 and MYH.
Authors contributions: D.Y. performed MettL3-14 activity assays. J.Y. performed assays of base excision repair. J.R.H. performed structural determinations of YTH in complex with DNA. T.H. and M.V. provided recombinant MettL3-MettL14 enzymes. S.C.A. and M.T.B performed GST pull-down assay. R.M.B. performed analysis on sequence conservation, participated in discussion throughout and assisted in preparing the manuscript. X.Z. and X.C. organized and designed the experimental scope of the study.

FUNDING

U.S. National Institutes of Health (NIH) [R35GM134744 to X.C., R01GM126412 to M.T.B.]; Cancer Prevention and Research Institute of Texas (CPRIT) [RR160029 to X.C. who is a CPRIT Scholar in Cancer Research]. Funding for open access charge: MD Anderson Cancer Center.
Conflict of interest statement. M.T.B. is a confounder of EpiCypher. Others declare no competing interests.

REFERENCES

1. Olivieri,M., Cho,T., Alvarez-Quilon,A., Li,K., Schellenberg,M.J., Zimmermann,M., Hustedt,N., Rossi,S.E., Adam,S., Melo,H. *et al.* (2020) A genetic map of the response to DNA damage in human cells. *Cell*, **182**, 481–496.
2. Xiang,Y., Laurent,B., Hsu,C.H., Nachtergaele,S., Lu,Z., Sheng,W., Xu,C., Chen,H., Ouyang,J., Wang,S. *et al.* (2017) RNA m(6)A methylation regulates the ultraviolet-induced DNA damage response. *Nature*, **543**, 573–576.
3. Zhang,C., Chen,L., Peng,D., Jiang,A., He,Y., Zeng,Y., Xie,C., Zhou,H., Luo,X., Liu,H. *et al.* (2020) METTL3 and N6-methyladenosine promote homologous recombination-mediated repair of DSBs by modulating DNA-RNA hybrid accumulation. *Mol. Cell*, **79**, 425–442.
4. Frye,M., Jaffrey,S.R., Pan,T., Rechavi,G. and Suzuki,T. (2016) RNA modifications: what have we learned and where are we headed? *Nat. Rev. Genet.*, **17**, 365–372.
5. Frye,M., Harada,B.T., Behm,M. and He,C. (2018) RNA modifications modulate gene expression during development. *Science*, **361**, 1346–1349.
6. Liu,J., Dou,X., Chen,C., Chen,C., Liu,C., Xu,M.M., Zhao,S., Shen,B., Gao,Y., Han,D. *et al.* (2020) N (6)-methyladenosine of chromosome-associated regulatory RNA regulates chromatin state and transcription. *Science*, **367**, 580–586.
7. Schibler,U., Kelley,D.E. and Perry,R.P. (1977) Comparison of methylated sequences in messenger RNA and heterogeneous nuclear RNA from mouse L cells. *J. Mol. Biol.*, **115**, 695–714.
8. Scully,R., Panday,A., Elango,R. and Willis,N.A. (2019) DNA double-strand break repair-pathway choice in somatic mammalian cells. *Nat. Rev. Mol. Cell. Biol.*, **20**, 698–714.
9. Barbieri,I., Tzelepis,K., Pandolfini,L., Shi,J., Millan-Zambrano,G., Robson,S.C., Aspris,D., Migliori,V., Bannister,A.J., Han,N. *et al.* (2017) Promoter-bound METTL3 maintains myeloid leukaemia by m(6)A-dependent translation control. *Nature*, **552**, 126–131.
10. Kuppers,D.A., Arora,S., Lim,Y., Lim,A.R., Carter,L.M., Corrin,P.D., Plaisier,C.L., Basom,R., Delrow,J.J., Wang,S. *et al.* (2019) N(6)-methyladenosine mRNA marking promotes selective translation of regulons required for human erythropoiesis. *Nat. Commun.*, **10**, 4596.
11. Li,Y., Xia,L., Tan,K., Ye,X., Zuo,Z., Li,M., Xiao,R., Wang,Z., Liu,X., Deng,M. *et al.* (2020) N(6)-methyladenosine co-transcriptionally directs the demethylation of histone H3K9me2. *Nat. Genet.*, **52**, 870–877.
12. Xu,W., Li,J., He,C., Wen,J., Ma,H., Rong,B., Diao,J., Wang,L., Wang,J., Wu,F. *et al.* (2021) METTL3 regulates heterochromatin in mouse embryonic stem cells. *Nature*, **591**, 317–321.
13. Liu,J., Gao,M., He,J., Wu,K., Lin,S., Jin,L., Chen,Y., Liu,H., Shi,J., Wang,X. *et al.* (2021) The RNA m(6)A reader YTHDC1 silences retrotransposons and guards ES cell identity. *Nature*, **591**, 322–326.
14. Huang,H., Weng,H., Zhou,K., Wu,T., Zhao,B.S., Sun,M., Chen,Z., Deng,X., Xiao,G., Auer,F. *et al.* (2019) Histone H3 trimethylation at lysine 36 guides m(6)A RNA modification co-transcriptionally. *Nature*, **567**, 414–419.

15. Song,G., Wang,G., Luo,X., Cheng,Y., Song,Q., Wan,J., Moore,C., Song,H., Jin,P., Qian,J. *et al.* (2021) An all-to-all approach to the identification of sequence-specific readers for epigenetic DNA modifications on cytosine. *Nat. Commun.*, **12**, 795.
16. Chelmicki,T., Roger,E., Teissandier,A., Dura,M., Bonneville,L., Rucli,S., Dossin,F., Fouassier,C., Lameiras,S. and Bourc'his,D. (2021) m(6)A RNA methylation regulates the fate of endogenous retroviruses. *Nature*, **591**, 312–316.
17. Geula,S., Moshitch-Moshkovitz,S., Dominissini,D., Mansour,A.A., Kol,N., Salmon-Divon,M., Hershkovitz,V., Peer,E., Mor,N., Manor,Y.S. *et al.* (2015) m6A mRNA methylation facilitates resolution of naive pluripotency toward differentiation. *Science*, **347**, 1002–1006.
18. Walsh,C.P., Chaillet,J.R. and Bestor,T.H. (1998) Transcription of IAP endogenous retroviruses is constrained by cytosine methylation. *Nat. Genet.*, **20**, 116–117.
19. Rowe,H.M., Jakobsson,J., Mesnard,D., Rougemont,J., Reynard,S., Aktas,T., Maillard,P.V., Layard-Liesching,H., Verp,S., Marquis,J. *et al.* (2010) KAP1 controls endogenous retroviruses in embryonic stem cells. *Nature*, **463**, 237–240.
20. Matsui,T., Leung,D., Miyashita,H., Maksakova,I.A., Miyachi,H., Kimura,H., Tachibana,M., Lorincz,M.C. and Shinkai,Y. (2010) Proviral silencing in embryonic stem cells requires the histone methyltransferase ESET. *Nature*, **464**, 927–931.
21. Morgan,H.D., Sutherland,H.G., Martin,D.I. and Whitelaw,E. (1999) Epigenetic inheritance at the agouti locus in the mouse. *Nat. Genet.*, **23**, 314–318.
22. Achwal,C.W., Iyer,C.A. and Chandra,H.S. (1983) Immunochemical evidence for the presence of 5mC, 6mA and 7mG in human, Drosophila and mealybug DNA. *FEBS Lett.*, **158**, 353–358.
23. Wu,T.P., Wang,T., Seetin,M.G., Lai,Y., Zhu,S., Lin,K., Liu,Y., Byrum,S.D., Mackintosh,S.G., Zhong,M. *et al.* (2016) DNA methylation on N(6)-adenine in mammalian embryonic stem cells. *Nature*, **532**, 329–333.
24. Xie,Q., Wu,T.P., Gimple,R.C., Li,Z., Prager,B.C., Wu,Q., Yu,Y., Wang,P., Wang,Y., Gorkin,D.U. *et al.* (2018) N(6)-methyladenine DNA modification in glioblastoma. *Cell*, **175**, 1228–1243.
25. Li,Z., Zhao,S., Nelakanti,R.V., Lin,K., Wu,T.P., Alderman,M.H., Guo,C., Wang,P., Zhang,M., Min,W. *et al.* (2020) N6-methyladenine in DNA antagonizes SATB1 in early development. *Nature*, **583**, 625–630.
26. Kouzine,F., Wojtowicz,D., Baranello,L., Yamane,A., Nelson,S., Resch,W., Kieffer-Kwon,K.R., Benham,C.J., Casellas,R., Przytycka,T.M. *et al.* (2017) Permanganate/S1 nuclease footprinting reveals non-B DNA structures with regulatory potential across a mammalian genome. *Cell Syst.*, **4**, 344–356.
27. Schiffers,S., Ebert,C., Rahimoff,R., Kosmatchev,O., Steinbacher,J., Bohne,A.V., Spada,F., Michalakis,S., Nickelsen,J., Muller,M. *et al.* (2017) Quantitative LC-MS provides no evidence for m(6) dA or m(4) dC in the genome of mouse embryonic stem cells and tissues. *Angew. Chem.*, **56**, 11268–11271.
28. Douvlataniotis,K., Bensberg,M., Lentini,A., Gylemo,B. and Nestor,C.E. (2020) No evidence for DNA N (6)-methyladenine in mammals. *Sci. Adv.*, **6**, eaay3335.
29. Musheev,M.U., Baumgartner,A., Krebs,L. and Niehrs,C. (2020) The origin of genomic N(6)-methyl-deoxyadenosine in mammalian cells. *Nat. Chem. Biol.*, **16**, 630–634.
30. Miura,G. (2020) Peaking at the right time. *Nat. Chem. Biol.*, **16**, 933–933.
31. Pennisi,E. (2020) Altered DNA base could play key role in pregnancy. *Science*, **369**, 495.
32. Forterre,P. and Grosjean,H. (2009) The Interplay between RNA and DNA modifications. In: Grosjean,H. (ed). *DNA and RNA Modification Enzymes: Structure, Mechanism, Function and Evolution*. Landes Bioscience, pp. 259–274.
33. Fedeles,B.I., Singh,V., Delaney,J.C., Li,D. and Essigmann,J.M. (2015) The AlkB family of Fe(II)/alpha-ketoglutarate-dependent dioxygenases: repairing nucleic acid alkylation damage and beyond. *J. Biol. Chem.*, **290**, 20734–20742.
34. Wolfe,A.D., Li,S., Goedderz,C. and Chen,X.S. (2020) The structure of APOBEC1 and insights into its RNA and DNA substrate selectivity. *NAR Cancer*, **2**, zcaa027.
35. Shen,Q., Zhang,Q., Shi,Y., Shi,Q., Jiang,Y., Gu,Y., Li,Z., Li,X., Zhao,K., Wang,C. *et al.* (2018) Tet2 promotes pathogen infection-induced myelopoiesis through mRNA oxidation. *Nature*, **554**, 123–127.
36. Lan,J., Rajan,N., Bizet,M., Penning,A., Singh,N.K., Guallar,D., Calonne,E., Li Greci,A., Bonvin,E., Deplus,R. *et al.* (2020) Functional role of Tet-mediated RNA hydroxymethylcytosine in mouse ES cells and during differentiation. *Nat. Commun.*, **11**, 4956.
37. Woodcock,C.B., Yu,D., Hajian,T., Li,J., Huang,Y., Dai,N., Correa,I.R. Jr, Wu,T., Vedadi,M., Zhang,X. *et al.* (2019) Human MettL3-MettL14 complex is a sequence-specific DNA adenine methyltransferase active on single-strand and unpaired DNA in vitro. *Cell Discov.*, **5**, 63.
38. Scharer,O.D. (2013) Nucleotide excision repair in eukaryotes. *Cold Spring Harb. Perspect Biol.*, **5**, a012609.
39. Hong,S., Hashimoto,H., Kow,Y.W., Zhang,X. and Cheng,X. (2014) The carboxy-terminal domain of ROS1 is essential for 5-methylcytosine DNA glycosylase activity. *J. Mol. Biol.*, **426**, 3703–3712.
40. Woodcock,C.B., Horton,J.R., Zhou,J., Bedford,M.T., Blumenthal,R.M., Zhang,X. and Cheng,X. (2020) Biochemical and structural basis for YTH domain of human YTHDC1 binding to methylated adenine in DNA. *Nucleic. Acids. Res.*, **48**, 10329–10341.
41. Hsiao,K., Zegzouti,H. and Goueli,S.A. (2016) Methyltransferase-Glo: a universal, bioluminescent and homogenous assay for monitoring all classes of methyltransferases. *Epigenomics*, **8**, 321–339.
42. Otwinowski,Z., Borek,D., Majewski,W. and Minor,W. (2003) Multiparametric scaling of diffraction intensities. *Acta Crystallogr. A*, **59**, 228–234.
43. McCoy,A.J., Grosse-Kunstleve,R.W., Adams,P.D., Winn,M.D., Storoni,L.C. and Read,R.J. (2007) Phaser crystallographic software. *J. Appl. Crystallogr.*, **40**, 658–674.
44. Headd,J.J., Echols,N., Afonine,P.V., Grosse-Kunstleve,R.W., Chen,V.B., Moriarty,N.W., Richardson,D.C., Richardson,J.S. and Adams,P.D. (2012) Use of knowledge-based restraints in phenix.refine to improve macromolecular refinement at low resolution. *Acta Crystallogr. D Biol. Crystallogr.*, **68**, 381–390.
45. Emsley,P. and Cowtan,K. (2004) Coot: model-building tools for molecular graphics. *Acta Crystallogr. D Biol. Crystallogr.*, **60**, 2126–2132.
46. Read,R.J., Adams,P.D., Arendall,W.B. 3rd, Brunger,A.T., Emsley,P., Joosten,R.P., Kleywegt,G.J., Krissinel,E.B., Lutteke,T., Otwinowski,Z. *et al.* (2011) A new generation of crystallographic validation tools for the protein data bank. *Structure*, **19**, 1395–1412.
47. Shaw,A.A. and Cadet,J. (1988) Formation of cyclopyrimidines via the direct effects of gamma radiation of pyrimidine nucleosides. *Int. J. Radiat. Biol.*, **54**, 987–997.
48. Rumora,A.E., Kolodziejczak,K.M., Malhowski Wagner,A. and Nunez,M.E. (2008) Thymine dimer-induced structural changes to the DNA duplex examined with reactive probes (dagger). *Biochemistry*, **47**, 13026–13035.
49. Wenke,B.B., Huiting,L.N., Frankel,E.B., Lane,B.F. and Nunez,M.E. (2013) Base pair opening in a deoxynucleotide duplex containing a cis-syn thymine cyclobutane dimer lesion. *Biochemistry*, **52**, 9275–9285.
50. Knips,A. and Zacharias,M. (2015) Influence of a cis,syn-cyclobutane pyrimidine dimer damage on DNA conformation studied by molecular dynamics simulations. *Biopolymers*, **103**, 215–222.
51. Mao,P., Smerdon,M.J., Roberts,S.A. and Wyrick,J.J. (2016) Chromosomal landscape of UV damage formation and repair at single-nucleotide resolution. *Proc. Natl. Acad. Sci. U.S.A.*, **113**, 9057–9062.
52. Mao,P., Brown,A.J., Esaki,S., Lockwood,S., Poon,G.M.K., Smerdon,M.J., Roberts,S.A. and Wyrick,J.J. (2018) ETS transcription factors induce a unique UV damage signature that drives recurrent mutagenesis in melanoma. *Nat. Commun.*, **9**, 2626.
53. Elliott,K., Bostrom,M., Filges,S., Lindberg,M., Van den Eynden,J., Stahlberg,A., Clausen,A.R. and Larsson,E. (2018) Elevated pyrimidine dimer formation at distinct genomic bases underlies promoter mutation hotspots in UV-exposed cancers. *PLoS Genet.*, **14**, e1007849.
54. Zhang,J., Baran,J., Cros,A., Guberman,J.M., Haider,S., Hsu,J., Liang,Y., Rivkin,E., Wang,J., Whitty,B. *et al.* (2011) International Cancer Genome Consortium Data Portal–a one-stop shop for cancer genomics data. *Database (Oxford)*, **2011**, bar026.

55. Lindberg,M., Bostrom,M., Elliott,K. and Larsson,E. (2019) Intragenomic variability and extended sequence patterns in the mutational signature of ultraviolet light. *Proc. Natl. Acad. Sci. U.S.A.*, **116**, 20411–20417.
56. Horn,S., Figl,A., Rachakonda,P.S., Fischer,C., Sucker,A., Gast,A., Kadel,S., Moll,I., Nagore,E., Hemminki,K. *et al.* (2013) TERT promoter mutations in familial and sporadic melanoma. *Science*, **339**, 959–961.
57. Huang,F.W., Hodis,E., Xu,M.J., Kryukov,G.V., Chin,L. and Garraway,L.A. (2013) Highly recurrent TERT promoter mutations in human melanoma. *Science*, **339**, 957–959.
58. Killela,P.J., Reitman,Z.J., Jiao,Y., Bettegowda,C., Agrawal,N., Diaz,L.A. Jr, Friedman,A.H., Friedman,H., Gallia,G.L., Giovanella,B.C. *et al.* (2013) TERT promoter mutations occur frequently in gliomas and a subset of tumors derived from cells with low rates of self-renewal. *Proc. Natl. Acad. Sci. U.S.A.*, **110**, 6021–6026.
59. Remke,M., Ramaswamy,V., Peacock,J., Shih,D.J., Koelsche,C., Northcott,P.A., Hill,N., Cavalli,F.M., Kool,M., Wang,X. *et al.* (2013) TERT promoter mutations are highly recurrent in SHH subgroup medulloblastoma. *Acta Neuropathol.*, **126**, 917–929.
60. Quaas,A., Oldopp,T., Tharun,L., Klingenfeld,C., Krech,T., Sauter,G. and Grob,T.J. (2014) Frequency of TERT promoter mutations in primary tumors of the liver. *Virchows. Arch.*, **465**, 673–677.
61. Huang,F.W., Bielski,C.M., Rinne,M.L., Hahn,W.C., Sellers,W.R., Stegmeier,F., Garraway,L.A. and Kryukov,G.V. (2015) TERT promoter mutations and monoallelic activation of TERT in cancer. *Oncogenesis*, **4**, e176.
62. Yuan,X., Liu,T. and Xu,D. (2020) Telomerase reverse transcriptase promoter mutations in thyroid carcinomas: implications in precision oncology-a narrative review. *Ann. Transl. Med.*, **8**, 1244.
63. Pierini,T., Nardelli,C., Lema Fernandez,A.G., Pierini,V., Pellanera,F., Nofrini,V., Gorello,P., Moretti,M., Arniani,S., Roti,G. *et al.* (2020) New somatic TERT promoter variants enhance the Telomerase activity in Glioblastoma. *Acta Neuropathol. Commun.*, **8**, 145.
64. Spiegl-Kreinecker,S., Lotsch,D., Neumayer,K., Kastler,L., Gojo,J., Pirker,C., Pichler,J., Weis,S., Kumar,R., Webersinke,G. *et al.* (2018) TERT promoter mutations are associated with poor prognosis and cell immortalization in meningioma. *Neuro. Oncol.*, **20**, 1584–1593.
65. Lorbeer,F.K. and Hockemeyer,D. (2020) TERT promoter mutations and telomeres during tumorigenesis. *Curr. Opin. Genet. Dev.*, **60**, 56–62.
66. Premi,S. and Brash,D.E. (2016) Chemical excitation of electrons: a dark path to melanoma. *DNA Repair (Amst.)*, **44**, 169–177.
67. Brash,D.E., Goncalves,L.C.P., Bechara,E.J.H. and Excited-State Medicine Working, G. (2018) Chemiexcitation and Its implications for disease. *Trends Mol. Med.*, **24**, 527–541.
68. Premi,S. (2020) Role of melanin chemiexcitation in melanoma progression and drug resistance. *Front. Oncol.*, **10**, 1305.
69. Horton,J.R., Woodcock,C.B., Opot,S.B., Reich,N.O., Zhang,X. and Cheng,X. (2019) The cell cycle-regulated DNA adenine methyltransferase CcrM opens a bubble at its DNA recognition site. *Nat. Commun.*, **10**, 4600.
70. Thompson,P.S. and Cortez,D. (2020) New insights into abasic site repair and tolerance. *DNA Repair (Amst.)*, **90**, 102866.
71. Liu,Z.J., Martinez Cuesta,S., van Delft,P. and Balasubramanian,S. (2019) Sequencing abasic sites in DNA at single-nucleotide resolution. *Nat. Chem.*, **11**, 629–637.
72. Masani,S., Han,L. and Yu,K. (2013) Apurinic/apyrimidinic endonuclease 1 is the essential nuclease during immunoglobulin class switch recombination. *Mol. Cell. Biol.*, **33**, 1468–1473.
73. Ogi,T., Limsirichaikul,S., Overmeer,R.M., Volker,M., Takenaka,K., Cloney,R., Nakazawa,Y., Niimi,A., Miki,Y., Jaspers,N.G. *et al.* (2010) Three DNA polymerases, recruited by different mechanisms, carry out NER repair synthesis in human cells. *Mol. Cell*, **37**, 714–727.
74. Takata,K., Arana,M.E., Seki,M., Kunkel,T.A. and Wood,R.D. (2010) Evolutionary conservation of residues in vertebrate DNA polymerase N conferring low fidelity and bypass activity. *Nucleic. Acids. Res.*, **38**, 3233–3244.
75. Zhao,Y., Gregory,M.T., Biertumpfel,C., Hua,Y.J., Hanaoka,F. and Yang,W. (2013) Mechanism of somatic hypermutation at the WA motif by human DNA polymerase eta. *Proc. Natl. Acad. Sci. U.S.A.*, **110**, 8146–8151.
76. Lee,Y.S., Gao,Y. and Yang,W. (2015) How a homolog of high-fidelity replicases conducts mutagenic DNA synthesis. *Nat. Struct. Mol. Biol.*, **22**, 298–303.
77. Haghdoost,S., Sjolander,L., Czene,S. and Harms-Ringdahl,M. (2006) The nucleotide pool is a significant target for oxidative stress. *Free Radic. Biol. Med.*, **41**, 620–626.
78. Kamath-Loeb,A.S., Hizi,A., Kasai,H. and Loeb,L.A. (1997) Incorporation of the guanosine triphosphate analogs 8-oxo-dGTP and 8-NH2-dGTP by reverse transcriptases and mammalian DNA polymerases. *J. Biol. Chem.*, **272**, 5892–5898.
79. Hanes,J.W., Thal,D.M. and Johnson,K.A. (2006) Incorporation and replication of 8-oxo-deoxyguanosine by the human mitochondrial DNA polymerase. *J. Biol. Chem.*, **281**, 36241–36248.
80. Pursell,Z.F., McDonald,J.T., Mathews,C.K. and Kunkel,T.A. (2008) Trace amounts of 8-oxo-dGTP in mitochondrial dNTP pools reduce DNA polymerase gamma replication fidelity. *Nucleic Acids Res.*, **36**, 2174–2181.
81. Freudenthal,B.D., Beard,W.A., Perera,L., Shock,D.D., Kim,T., Schlick,T. and Wilson,S.H. (2015) Uncovering the polymerase-induced cytotoxicity of an oxidized nucleotide. *Nature*, **517**, 635–639.
82. Wang,S., Song,Y., Wang,Y., Li,X., Fu,B., Liu,Y., Wang,J., Wei,L., Tian,T. and Zhou,X. (2017) The m(6)A methylation perturbs the Hoogsteen pairing-guided incorporation of an oxidized nucleotide. *Chem. Sci.*, **8**, 6380–6388.
83. Colussi,C., Parlanti,E., Degan,P., Aquilina,G., Barnes,D., Macpherson,P., Karran,P., Crescenzi,M., Dogliotti,E. and Bignami,M. (2002) The mammalian mismatch repair pathway removes DNA 8-oxodGMP incorporated from the oxidized dNTP pool. *Curr. Biol.*, **12**, 912–918.
84. Ni,T.T., Marsischky,G.T. and Kolodner,R.D. (1999) MSH2 and MSH6 are required for removal of adenine misincorporated opposite 8-oxo-guanine in S. cerevisiae. *Mol. Cell*, **4**, 439–444.
85. van Loon,B. and Hubscher,U. (2009) An 8-oxo-guanine repair pathway coordinated by MUTYH glycosylase and DNA polymerase lambda. *Proc. Natl. Acad. Sci. U.S.A.*, **106**, 18201–18206.
86. Fowler,R.G., White,S.J., Koyama,C., Moore,S.C., Dunn,R.L. and Schaaper,R.M. (2003) Interactions among the Escherichia coli mutT, mutM, and mutY damage prevention pathways. *DNA Repair (Amst.)*, **2**, 159–173.
87. Ushijima,Y., Tominaga,Y., Miura,T., Tsuchimoto,D., Sakumi,K. and Nakabeppu,Y. (2005) A functional analysis of the DNA glycosylase activity of mouse MUTYH protein excising 2-hydroxyadenine opposite guanine in DNA. *Nucleic. Acids. Res.*, **33**, 672–682.
88. Zhang,X., Blumenthal,R.M. and Cheng,X. (2021) A role for N6-methyladenine in DNA damage repair. *Trends Biochem. Sci.* **46**, 175–183.
89. Patil,D.P., Pickering,B.F. and Jaffrey,S.R. (2018) Reading m(6)A in the Transcriptome: m(6)A-binding proteins. *Trends Cell. Biol.*, **28**, 113–127.
90. Xu,C., Wang,X., Liu,K., Roundtree,I.A., Tempel,W., Li,Y., Lu,Z., He,C. and Min,J. (2014) Structural basis for selective binding of m6A RNA by the YTHDC1 YTH domain. *Nat. Chem. Biol.*, **10**, 927–929.
91. Dai,X., Wang,T., Gonzalez,G. and Wang,Y. (2018) Identification of YTH domain-containing proteins as the readers for N1-methyladenosine in RNA. *Anal. Chem.*, **90**, 6380–6384.
92. Liu,Y., Freeman,A.D.J., Declais,A.C., Wilson,T.J., Gartner,A. and Lilley,D.M.J. (2015) Crystal structure of a eukaryotic GEN1 resolving enzyme bound to DNA. *Cell Rep.*, **13**, 2565–2575.
93. Tsutakawa,S.E., Classen,S., Chapados,B.R., Arvai,A.S., Finger,L.D., Guenther,G., Tomlinson,C.G., Thompson,P., Sarker,A.H., Shen,B. *et al.* (2011) Human flap endonuclease structures, DNA double-base flipping, and a unified understanding of the FEN1 superfamily. *Cell*, **145**, 198–211.
94. Lilley,D.M.J. (2017) Holliday junction-resolving enzymes-structures and mechanisms. *FEBS Lett.*, **591**, 1073–1082.
95. Paul,D., Mu,H., Zhao,H., Ouerfelli,O., Jeffrey,P.D., Broyde,S. and Min,J.H. (2019) Structure and mechanism of pyrimidine-pyrimidone (6-4) photoproduct recognition by the Rad4/XPC nucleotide excision repair complex. *Nucleic Acids Res.*, **47**, 6015–6028.
96. Zhang,M., Yang,S., Nelakanti,R., Zhao,W., Liu,G., Li,Z., Liu,X., Wu,T., Xiao,A. and Li,H. (2020) Mammalian ALKBH1 serves as an N(6)-mA demethylase of unpairing DNA. *Cell Res.*, **30**, 197–210.
97. Pukkila,P.J., Peterson,J., Herman,G., Modrich,P. and Meselson,M. (1983) Effects of high levels of DNA adenine methylation on methyl-directed mismatch repair in Escherichia coli. *Genetics*, **104**, 571–582.